Investigations on Retinal Pigment Epithelial Damage at Laser Irradiation in the Lower Microsecond Time Regime

Eric Seifert,[1] Svenja Rebecca Sonntag,[2] Philipp Kleingarn,[1] Dirk Theisen-Kunde,[1] Salvatore Grisanti,[2] Reginald Birngruber,[1,3] Yoko Miura,[2,3] and Ralf Brinkmann[1,3]

[1]Medical Laser Center Lübeck, Lübeck, Germany
[2]Department of Ophthalmology, University of Lübeck, Lübeck, Germany
[3]Institute of Biomedical Optics, University of Lübeck, Lübeck, Germany

Correspondence: Ralf Brinkmann, Medizinisches Laserzentrum Lübeck GmbH, Peter-Monnik-Weg 4, 23562 Lübeck, Germany; ralf.brinkmann@uni-luebeck.de.

Received: July 12, 2020
Accepted: February 1, 2021
Published: March 23, 2021

Citation: Seifert E, Sonntag SR, Kleingarn P, et al. Investigations on retinal pigment epithelial damage at laser irradiation in the lower microsecond time regime. *Invest Ophthalmol Vis Sci.* 2021;62(3):32. https://doi.org/10.1167/iovs.62.3.32

Purpose. New lasers with a continuous wave power exceeding 15 W are currently investigated for retinal therapies, promising highly localized effects at and close to the Retinal Pigment Epithelium (RPE). The goal of this work is to evaluate mechanisms and thresholds for RPE cell damage by means of pulse durations up to 50 µs.

Methods. A diode laser with a wavelength of 514 nm, a power of 15 W, and adjustable pulse durations between 2 µs and 50 µs was used. Porcine RPE-choroidal explants (ex vivo) and chinchilla bastard rabbits (in vivo) were irradiated to determine threshold radiant exposures for RPE damage $\bar{H}_{Cell}$ by calcein vitality staining and fluorescence angiography, respectively. Thresholds for microbubble formation (MBF) $\bar{H}_{MBF}$ were evaluated by time-resolved optoacoustics. Exemplary histologies support the findings.

Results. $\bar{H}_{MBF}$ is significantly higher than $\bar{H}_{Cell}$ at pulse durations $\geq$ 5 µs ($P < 0.05$) ex vivo, while at 2 µs, no statistically significant difference was found. The ratios between $\bar{H}_{MBF}$ and $\bar{H}_{Cell}$ increase with pulse duration from 1.07 to 1.48 ex vivo and 1.1 to 1.6 in vivo, for 5.2 and 50 µs.

Conclusions. Cellular damage with and without MBF related disintegration are both present and very likely to play a role for pulse durations $\geq$ 5 µs. With the lower µs pulses, selective RPE disruption might be possible, while higher values allow achieving spatially limited thermal effects without MBF. However, both modi require a very accurate real-time dosing control in order to avoid extended retinal disintegration in this power range.

Keywords: RPE, retina, SRT, photocoagulation, thermal damage, thermomechanical damage, microbubble formation, photodisruption, threshold irradiance, rabbits

A variety of laser systems with different wavelengths, pulse durations, and fluences are used for therapeutic retinal applications. The main absorber of the laser energy for all wavelengths in the visible spectrum are the micrometer-sized melanin granula within the RPE and the choroid, acting as heat sources.[1,2] For laser photocoagulation (LPC) with pulse durations in the range of 20 ms to 500 ms, the RPE and choroid can be assumed as uniformly absorbing layers. Owing to heat flow during and shortly after laser irradiation, the neural retina in front of the RPE is also heated. The thermal damage and its extension increase with temperature and time elevated temperatures are present and can be well described with the theory of Arrhenius.[2,3] An overall mean threshold temperature for thermal damage was measured to be 53 ± 2°C by means of pulse durations between 0.1 and 1 seconds on cultured RPE cells.[4] During clinical LPC, temperatures between 70°C and 85°C were measured for ophthalmoscopically barely visible lesions.[5] Using optical coherence tomography (OCT) within one hour after treatment showed tissue alterations at even lower temperatures.[6]

If pulse durations in the nanosecond to lower microsecond time regime are used, the granula structure of the absorbers need to be considered since the thermal relaxation time of a single (spherical) melanosome of 1 µm in diameter is only about 420 ns,[7] and for small 0.6-µm melanosomes, it is about 100 ns.[8] In selective retina therapy (SRT) using pulse durations of 1.7 µs and a peak power around 100 W, temperatures far exceed 100°C, and vaporization at the melanosomes at about 140°C was proven.[9,10] Consequently, microbubble formation (MBF) sets in.[7,11,12] The rapid expansion of the multiple bubbles with intracellular volume increase going along mechanically disrupts the cell membrane, and thus thermomechanical cell disintegration becomes the primary damage process, without signs of thermal damage.[7,13] This photodisintegration is used to selectively damage the RPE in SRT[14–19] with repetitive 1.7 µs pulses and in 2RT (Ellex Inc., Mawson Lakes, Australia)[20] using a single 3 ns pulse. If the vaporization threshold energy is exceeded by a factor of 2 or more, the photoreceptors and the neural retina get also affected, which is indicated by ophthalmoscopically visible lesions.[21] Further increasing the laser energy even leads to visible bubble formation at the retina, observed with repetitive 200-ns pulses slightly above radiant exposure for ophthalmic visibility.[22] In order to eliminate this risk, automatic feedback

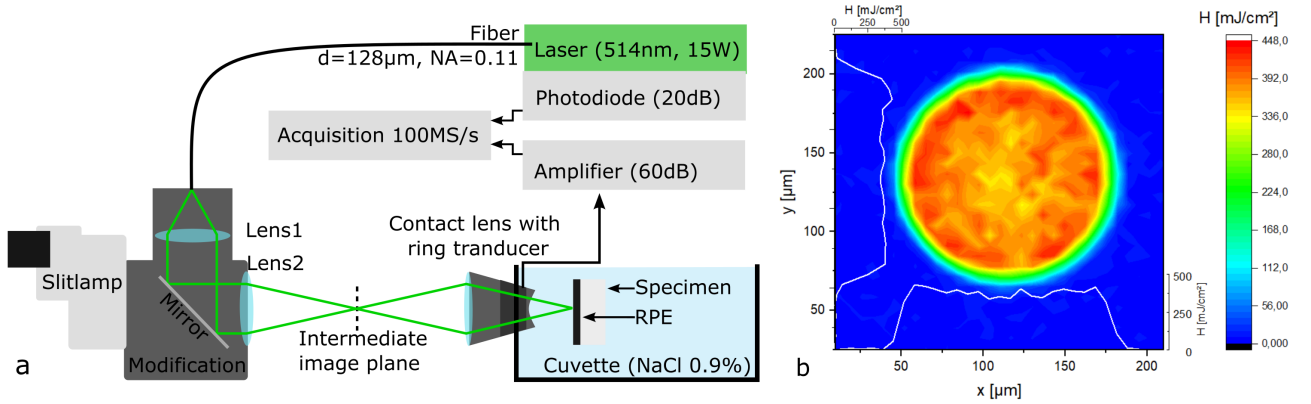

Figure 1. (**a**) Schematic of the experimental setup (ex vivo). (**b**) Spatial beam profile in the intermediate image plane with peak to mean ratio (IMF) of 1.2 exemplary for a 12-µs laser pulse with a pulse energy of 49 µJ. Beam profile cross section (white lines) display the radiant exposure across the center.

systems are demanded. First an optoacoustic method was developed to detect MBF.[14,23] Later, optical techniques analyzing the reflected treatment light in real-time were used to cease laser radiation applied in a pulse energy ramp mode after MBF.[24,25] Further m-mode Optical Coherence Tomography (OCT) was also employed for MBF detection by fringe washout.[26,27]

Very recently, new compact laser sources with high continuous wave power >15 W and variable pulse duration from 2 µs to 50 µs were investigated for retinal therapies.[28] With these new high-power laser sources, for the first time, subvisible effects with repetitive micropulses,[3,29–31] pure thermal tissue damage as in LPC, and MBF-related thermomechanical effects as in SRT might be accessed with just one laser system, only by adjusting the pulse duration and pulse repetition rate appropriately. However, so far, only few studies have investigated the transition regime from thermomechanical to thermal effects in the 2- to 50-µs pulse regime, accessible with this high power.[11,12]

The aim of this work is to investigate the laser damage thresholds and damage mechanisms in this time domain. Therefore, a novel optoacoustic approach was developed to identify the exact time MBF takes place during the application of one single microsecond pulse in order to accurately determine the radiant exposure for MBF. In order to investigate these effects, porcine RPE explants and chinchilla bastard rabbits were used as a model. Comparing the radiant exposures for cell damage with those of MBF provides detailed insight into the damage mechanisms as a function of the pulse duration and radiant exposure.

Materials and Methods

Hardware and Optics

A 15-W diode laser (A.R.C. Laser GmbH, Nürnberg, Germany) with a wavelength of 514 nm and adjustable pulse duration from 2 to 50 µs duration was used. The treatment light and aiming laser light (650 nm) were transmitted by an optical fiber with a core diameter of 128 µm (NA = 0.11), as shown in Figure 1a. The fiber was coupled to a modified slit lamp. The optical system consisted of two planoconvex lenses with a focal length of 100 mm each (Fig. 1a, lens 1 and lens 2) and a dichroic mirror being high reflective under 45° for the diode and pilot laser radiation. Thus, the fiber tip was imaged to an intermediate image plane with a magnification factor of 1. A maximum power of 11 W could be obtained in front of the slit lamp.

The laser pulse shapes (laser power over time) were acquired with a photodiode (PDA10A; Thorlabs, Inc., Newton, New Jersey, USA) during all experiments. Prior to the tissue experiments, the pulse energies for different pulse durations and laser powers were measured with an energy meter (EnergyMax USB J-10MB LE; Coherent, Santa Clara, California, USA) in front of the slit lamp. The laser pulse shape acquired with the diode was calibrated to the pulse energy. Further, the intensity modulation factor (IMF), defining the ratio of peak to mean radiant exposure across the beam profile, was determined with a CCD beam profiler BC106VIS (Thorlabs, Inc.) in the intermediate image plane (Fig. 1a) by use of an image magnification of 10. Value of IMF around 1.2 had been achieved for all pulse durations, and an exemplary beam profile of a 12-µs pulse is shown in Figure 1b. This IMF indicates an almost top hat beam profile. In all experiments, a Mainster contact lens (Ocular Instruments Inc, Bellevue, Washington, USA) imaged the intermediate image plane to the RPE. In the ex vivo experiments, the RPE and the concave part of the contact lens were placed inside a cuvette filled with ringer solution (0.9% NaCl). An annular 1-MHz ultrasonic transducer was embedded in the contact lens (Medical Laser Center Lübeck, Lübeck, Germany). The transducer signal was amplified by 60 dB (Panametrics—NDT Ultrasonic Preamplifier; Olympus, Tokyo, Japan) and acquired by a digitizer card with a sampling rate of 100 MS/s (GaGe Octopus; Dynamic Signals LLC, Lockport, Illinois, USA).

The radiant exposures H for each pulse, for RPE cell damage, for ophthalmic visibility, and for MBF presented in this work were calculated by

$$H_{Pulse} = \frac{E_{Pulse}}{A} \cdot IMF \cdot T$$

$$H_{MBF} = \frac{\int_{t=0}^{t_{MBF}} P_P(t)\,dt}{A} \cdot IMF \cdot T$$

$$H_{Cell} = \frac{E_{Cell}}{A} \cdot IMF \cdot T$$

$$H_{Opb} = \frac{E_{Opb}}{A} \cdot IMF \cdot T$$

with the laser pulse energy E_{Pulse}, the threshold energies for cell damage E_{Cell} and ophthalmoscopic visibility E_{Opb}, the

Investigative Ophthalmology & Visual Science

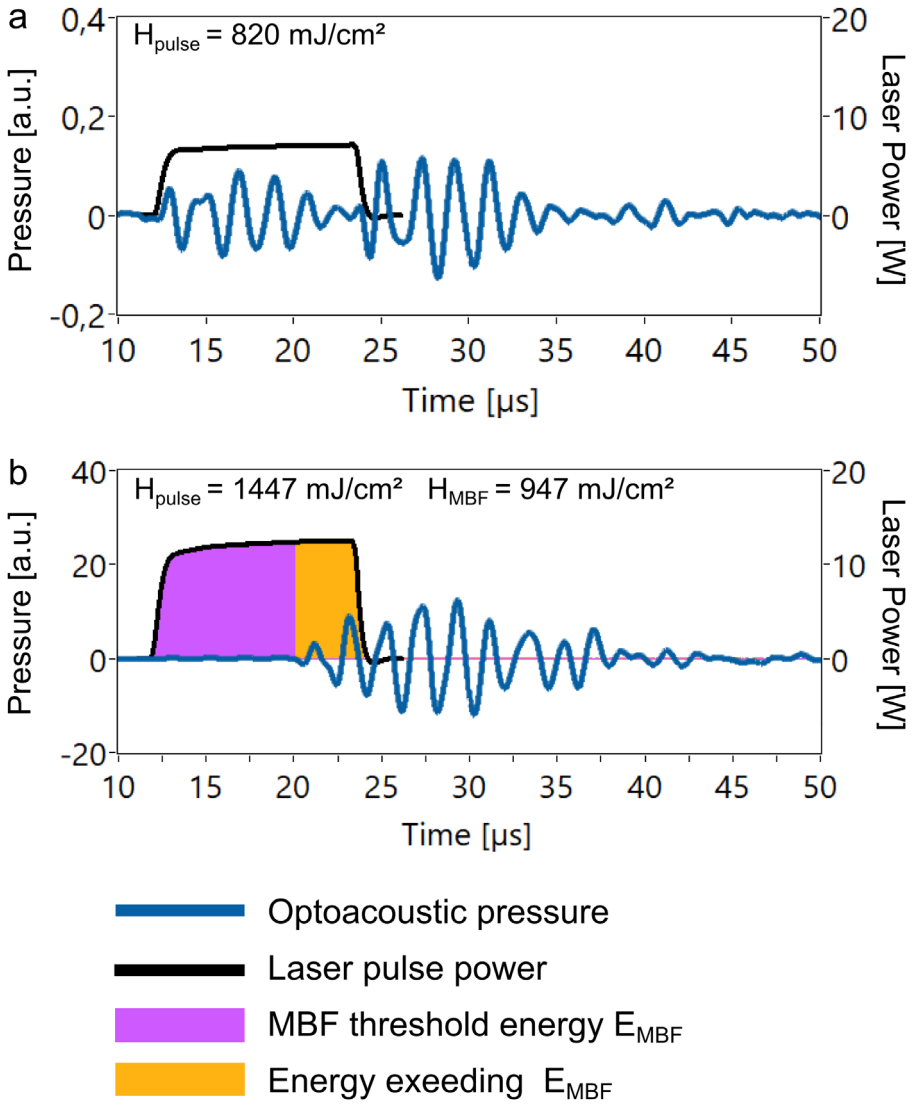

Figure 2. Examples of optoacoustic transients (*blue*) *below* (**a**) and *above* (**b**) the threshold for MBF. The laser pulse is displayed in *black*. The laser pulse was shifted temporally by the acoustic transit time for better understandability. The *purple area* under the pulse represents the laser pulse energy until threshold for MBF, the *orange area* represents the laser pulse energy for additional heating. Note the 100 times larger pressure amplitudes for MBF in (**b**).

laser pulse power $P_P(t)$, the area A of the spot, the intensity modulation factor IMF, and the starting time for MBF t_{MBF}. The direct transmission T is the proportion of the laser light emitted from the slit lamp, which reaches the target area. The direct transmission is approximately $T = 1$ in the ex vivo experiments performed in a cuvette. A value of $T = 0.5$ was used for rabbits according to findings of former studies owing to the opacity of the anterior eye media.[32] To get an interindividual threshold $\bar{H}$, the mean of the local thresholds H was calculated. The ratio of threshold radiant exposures for MBF ($\bar{H}_{MBF}$) to that for cell damage ($\bar{H}_{Cell}$) is called damage ratio $DR = (\bar{H}_{MBF}/\bar{H}_{Cell})$. In the case of simultaneous occurrence of cell damage and microbubble detection, the damage ratio had a value of 1.

Single-Pulse Optoacoustic Microbubble Detection

We present a method to determine MBF and its exact nucleation time by applying a single-laser pulse only, in contrast to previous work. Therefore, the acoustic transients were processed as follows: in the first step, the relevant signal components were cleared from noise by the application of a bandpass filter with the upper cutoff frequency of 800 kHz and a lower cutoff frequency of 500 kHz. For pulse durations of at least 5 µs, two acoustic transients could be identified, related to the strong temperature gradients initiating thermoelastic heating and cooling at the beginning and end of the pulse. The time between the onset times of both transients was identical to the pulse duration. In Figures 2a and 2b, the laser pulse was shifted temporarily by the acoustic transit time, defined as the time the pressure wave needs to travel from the specimen to the transducer, in order to illustrate this observation. The amplitudes of both transients were similar to each other, as shown in Figure 2a with $H_{pulse} = 820\,\mathrm{mJ/cm^2}$. The amplitude of thermoelastic transients rose proportionally to the pulse energy. Figure 2b displays an irradiation of $H_{pulse} = 1447\,\mathrm{mJ/cm^2}$, 76% higher compared to the one shown in Figure 2a. A third acoustic transient was observed between the thermoelastic transients with an amplitude 100 times larger than those ones at pulse

beginning and end. This transient can be associated with MBF taking place after about 8 µs at a radiant exposure of $H_{MBF} = 947\,mJ/cm^2$. The pulse energy applied to the onset time point of the second transient was the threshold pulse energy E_{MBF} for MBF (Fig. 2b, purple area).

It must be noted that it was not possible to identify the point in time of MBF at a pulse duration of 2 µs because the optoacoustic transient of the thermoelastic expansion was still present when MBF took place. For this pulse duration, microbubble detection was determined by the nonlinear increase of the optoacoustic amplitude only.

Ex Vivo Experiments

Tissue explants of freshly enucleated porcine eyes consisting of RPE, Bruch's membrane, the choroid, and the sclera were used. The explants had low pigmentation. The explant was placed inside a cuvette filled with physiologic saline solution. Pulse durations of 2 µs, 5 µs, 7 µs, 12 µs, 20 µs, 35 µs, and 50 µs were applied on the RPE. One pulse was applied per spot. The pulse energy was varied with every spot.

Moving the specimen within the cuvette and the slit lamp accordingly offered the ability to vary the spot magnification. For all pulse durations, a spot magnification factor of 1.025 was used except for 2 µs, where the magnification was reduced to 0.51 (65 µm) to increase the radiant exposure.

Calcein viability assay was used to evaluate RPE cell damage. The nonfluorescent dye Calcein-AM (3 µM) was applied to the RPE 30 minutes after irradiation for 15 minutes. The tissue was then rinsed with PBS and mounted on a microscope slide, and fluorescence microcopy was performed with an Eclipse Ti-E fluorescence microscope (Nikon Instruments, Tokyo, Japan), using a filter for fluorescein (range of excitation wavelength 465–495 nm, cutoff 505 nm, range of detection wavelength 515–555 nm). Green fluorescence displays vital cells, while hypofluorescence or complete absence of fluorescence indicates dead or missing cells. For the data to be classified as damaged, we defined a minimum of seven cells to be hypofluorescent within a region that was known to be irradiated. For the data to be classified as undamaged, hyperfluorescence must be identifiable at a position that was known to be treated.

In Vivo Experiments

Chinchilla gray rabbits were used in this study (permission reference number: V242-12638/2018 (31-4/18)). Rabbits of similar age (9 months) and similar weight (3 kg) were used. The animal experiments were in adherence with the ARVO guidelines. The rabbits were anesthetized with ketamine (25 mg/kg) and medetomidin (0.25 mg/kg) via an intramuscular injection. The pupils were dilated with eye drops containing phenylephrine and tropicamid, and the ocular surface was locally anesthetized with oxybuprocain hydrochlorid (Conjuncain, Laval, Quebec, Canada). The rabbit was placed in a stabilized position in front of the slit lamp. The contact lens with embedded ultrasonic transducer was placed on the cornea with an index matching gel (Methocel 2%, OmniVision GmbH, Puchheim, Germany). The eye not under treatment was closed to prevent drying. The anatomic and optical properties of the eye led to a reduced spot size of 85 µm (66% of spot size in intermediate image plane) with the Mainster contact lens used.[33]

An irradiation pattern with predefined radiant exposures and pulse durations was applied to the RPE. The pattern was repeated three times. Ophthalmoscopically visible marker spots (11 *W*, 50 µs) ensured correct spot assignment during the evaluation. One hour after treatment, fluorescein angiography (FA) was performed, which is an established method to diagnose the blood-retina-barrier properties of the RPE.[34] Data were classified as unevaluable if doubts about the state of cell damage of the exact spot assignment arose. To be classified as undamaged (FA nonvisible), a retinal region must be clearly visible and neighboring spots must be placed correctly. To be classified as damaged (FA visible), fluorescence must be identifiable at a position that was known to be treated.

Histology

For histologic evaluation, three animals (six eyes) were treated as described above, including laser irradiation and retinal imaging except FA, to potentially not to interfere with the histologic dyes, and euthanized with pentobarbital (200 mg/kg body weight) injected from the marginal ear vein one hour after treatment. Immediately after euthanasia, both eyes were enucleated, cleaned away from the extraocular tissues, and fixed in a Margo fixative solution (1% formaldehyde + 1.25% glutaraldehyde) for 24 hours at 4C. Anterior segment of the eye, including cornea, iris, and lens, and the vitreous body were then resected through a circle incision at the pars plana. Under a stereo microscope, the irradiated retinal area was recognized (marker spots were mostly detectable), and a small piece of the tissue including this area (from retina to sclera, about 5 × 5 mm) was resected with a razor blade. The tissue was then embedded in paraffin, and consecutive 5-µm-thick sections were prepared through the examined area and stained with hematoxylin and eosin (HE). Stained specimen were observed and recorded with a light microscope (Eclips Ti; Nikon, Tokyo, Japan).

Statistical Analysis

H_{Cell} and H_{MBF} were compared by *t*-test. Statistic software (OriginLab Corporation, Northampton Massachusetts, USA) was utilized to perform a nonpaired *t*-test. A *P* value less than 0.05 was defined as significant. For in vivo data, a *t*-test could not be made since the number of data was too low. An additional 76 evaluable eyes (minimum of 38 rabbits) would have been required to obtain a statistical power of 0.95, which by far would have exceeded the scope of this study.

Results

Ex Vivo Experiments

In the ex vivo experiments, 2310 data sets consisting of irradiated spots with the according optoacoustic transients were obtained. Figure 3a shows a calcein-stained fluorescence microscopy image with different pulse durations in six columns, next to four columns of strong marker lesions. Figures 3b–d display selected laser pulses with the applied radiant exposure and corresponding acoustic transients for a laser pulse duration of 35 µs for an undamaged spot (Fig. 3b), as well as hypofluorescent spots without (Fig. 3c) and with MBF (Fig. 3d). The mean values for $\bar{H}_{Cell}$ and $\bar{H}_{MBF}$ for each pulse duration are shown in Table 1. It was found that the mean $\bar{H}_{Cell}$ was lower than the mean

Investigative Ophthalmology & Visual Science

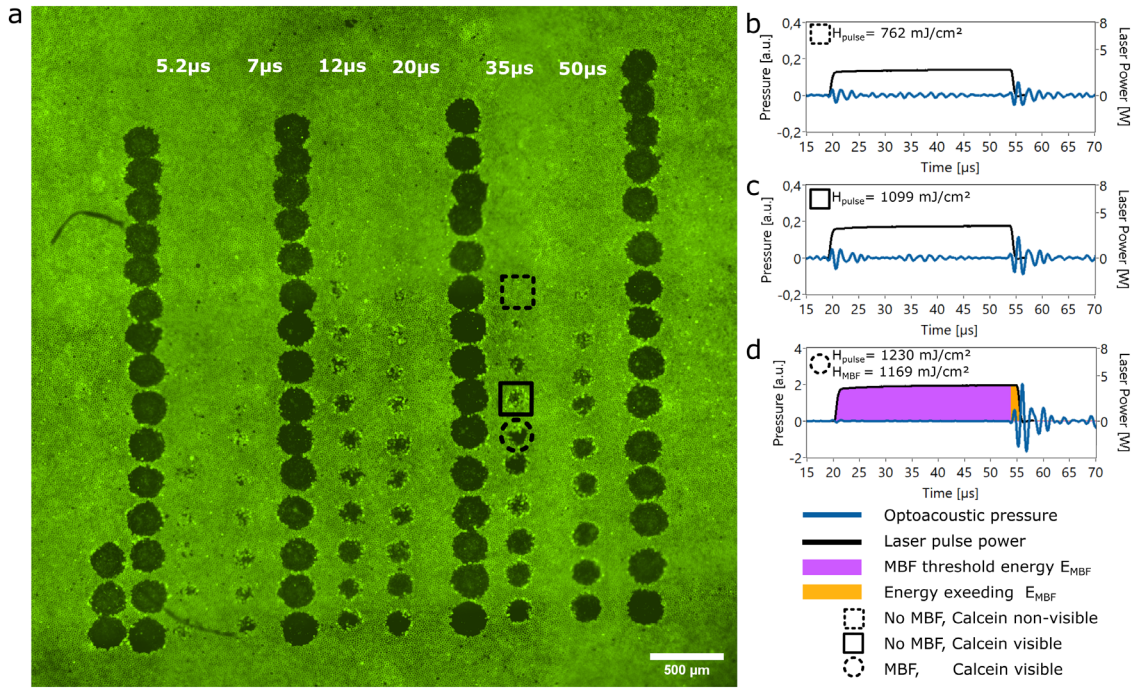

Figure 3. (**a**) Fluorescence microscopic image of a calcein viability stained probe. Four columns of strong marker lesions were placed, in between six columns of spots with different pulse durations in each column. Laser energy was always increased from the upper to the lower part of the column. In the 35-µs column, three spots are highlighted and their laser pulse shapes and acoustic transients are shown in subfigures b–d. The dashed square (**b**) displays an undamaged area, the last in the column. The spot highlighted with the solid square is the last spot without detectable MBF (**c**). The spot with the dashed circle is the first spot with MBF (**d**), indicated by the 20 times higher acoustic amplitude compared to (**a**) and (**b**).

Table 1. Ex Vivo Threshold Radiant Exposures

τ (µs)	N_{Cell}	$\bar{H}_{Cell}$ (mJ/cm²)	N_{MBF}	τ_{MBF} (µs)	$\bar{H}_{MBF}$ (mJ/cm²)	DR
2*	21	259	21	Unknown	257*	0.99*
5.2	24	465	111	5.4	496	1.07
7	22	505	88	6.8	564	1.12
12	22	630	64	11.9	723	1.15
20	22	752	27	19.7	943	1.25
35	22	955	18	34.9	1253	1.31
50	21	1198	6	48.1	1770	1.48

DR increases with increasing pulse duration.
*At a pulse duration of 2 µs, MBF was determined by strong amplitudes.

Table 2. In Vivo Threshold Radiant Exposures for Cell Damage, MBF, and Ophthalmoscopic Visibility

τ (µs)	$\bar{H}_{Cell}$ (mJ/cm²)	$\bar{t}_{MBF}$ (µs)	$\bar{H}_{MBF}$ (mJ/cm²)	$\bar{H}_{Opb}$ (mJ/cm²)	DR H_{MBF}/H_{Cell}
5.2	311	4.8	344	565	1.11
12	524	11.7	594	976	1.13
20	636	19.2	831	1184	1.3
50	1041	47.4	1662	2127	1.6

$\bar{H}_{MBF}$ for pulse durations from 5 to 50 µs ($P < 0.05$). At 2 µs, the threshold values did not show significant difference (damage ratio [DR] = 1.03, $P = 0.8$). Based on these results, it can be assumed that MBF is the primary cell damage mechanism at a pulse duration of 2 µs.

Figure 4 displays the thresholds over pulse duration. The threshold values for cell damage and MBF were fitted with a function of the form $H = A\,\tau^b$ for values of τ in microseconds. For cell damage, the parameters are $A_{Cell} = 220$ and $b_{Cell} = 0.41$. For MBF, the parameters are $A_{MBF} = 204$ and $b_{MBF} = 0.51$.

In Vivo Experiments

Overall, 2290 data sets were acquired from irradiations of 11 rabbits (22 eyes, 59 irradiation patterns). The values for $\bar{H}_{Cell}$ and $\bar{H}_{MBF}$ are shown in Table 2. In Figures 5a and 5b, an exemplary fundus image and the corresponding FA image are displayed. Surrounded by U-shaped pattern of marker lesions, four columns of lesions were applied with different pulse durations and radiant exposures, respectively. Exemplary few spots with pulse durations of 5.2 and 12 µs are selected and shown with their laser pulse shapes and acoustic transients in Figures 5c–f and Figures 5g–j, respectively. Subfigures c and g display signals associated with an undamaged region. Subfigures d and h display signals associated with initial retinal damage (local threshold) under the absence of MBF. Subfigures e and i display signals associated with cell damage and MBF (local threshold). Finally, subfigures f and j display signals associated with ophthalmoscopic visibility during treatment.

It can further be noticed that $\bar{H}_{MBF}$ and $\bar{H}_{Cell}$ of shorter pulses are lower than those of longer pulses. This can be explained with head conduction during irradiation.

As in the ex vivo experiments, the DR has been found to increase with increasing pulse duration, as shown in Table 2. Figure 6 shows $\bar{H}_{MBF}$, $\bar{H}_{Cell}$, and $\bar{H}_{Opb}$ with its fitted functions. The parameters for cell damage are $A_{Cell} = 145$ and $b_{Cell} =$

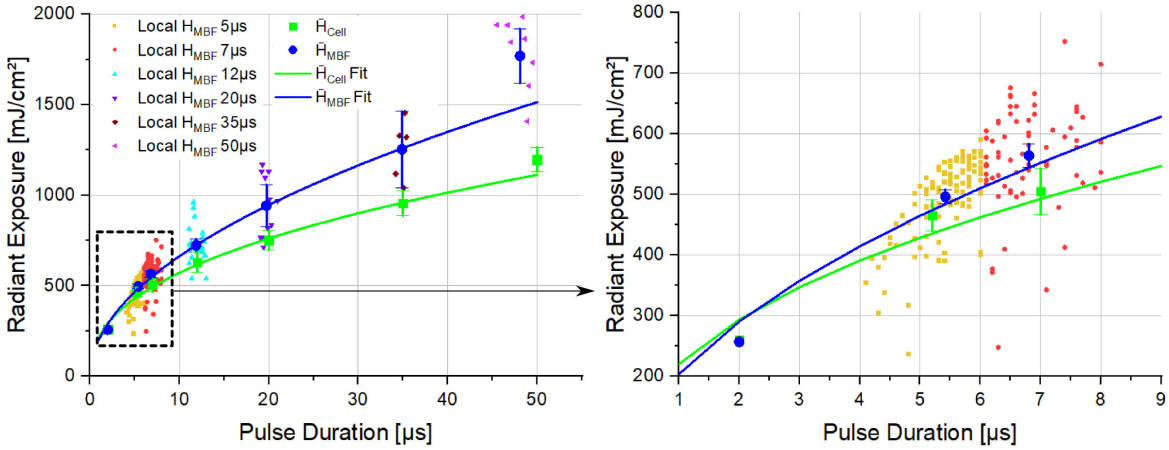

Figure 4. Threshold radiant exposures over pulse duration for ex vivo specimen. Points indicate local H_{MBF} values used for calculation of the interindividual $\bar{H}_{MBF}$ value. Larger points with error bar display $\bar{H}_{Cell}$ (*green rectangles*) and $\bar{H}_{MBF}$ (*blue dots*). *Error bars* show the 95% confidence interval. The *dashed area* is magnified in the *right plot*.

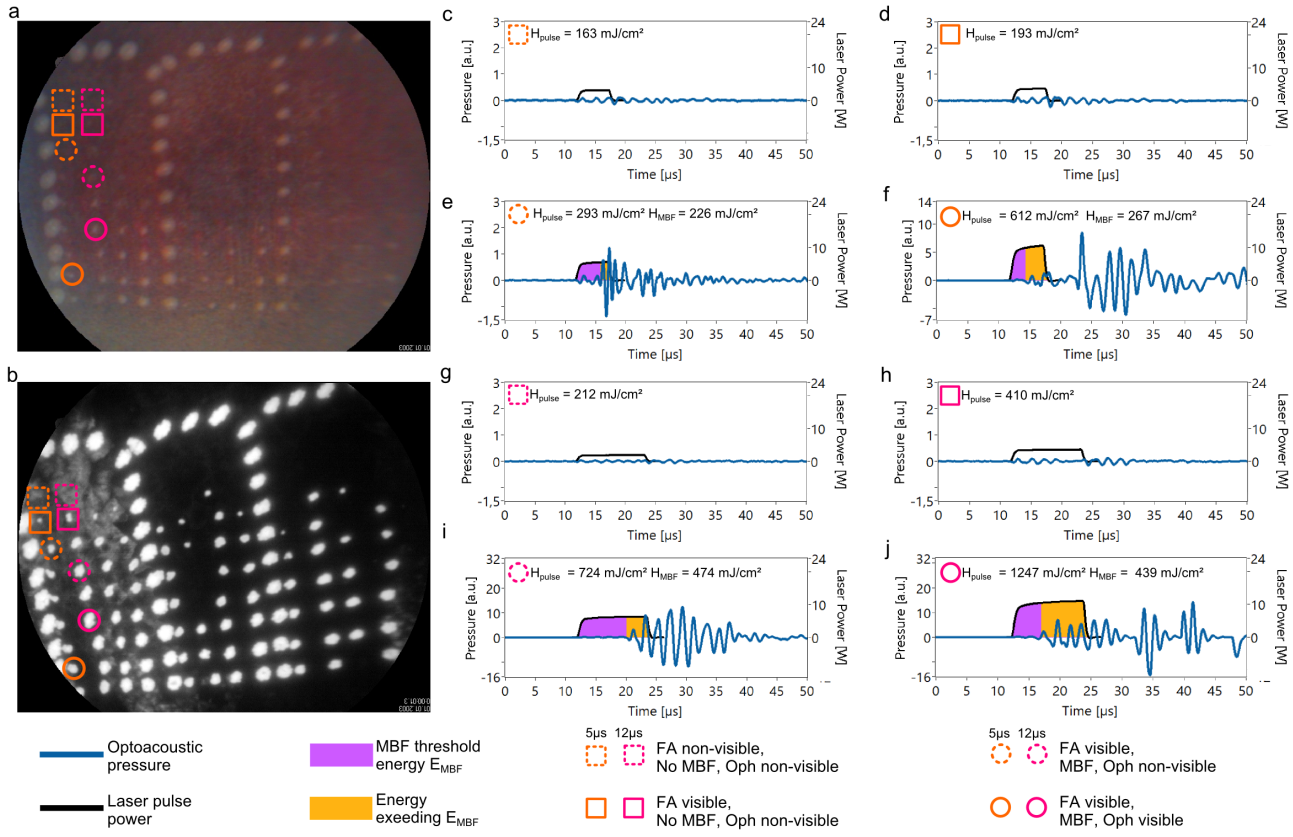

Figure 5. (**a**) Fundus image of a treated region. (**b**) FA image corresponding to subfigure a. The larger bright spots in U-shaped pattern are marker lesions. The lesions used for the evaluation were applied within this pattern. Circles and rectangles mark the region of origin of the signals displayed in subfigures c–j. (c–j) Laser power and acoustic pressure for different degrees of cell damage including no cell damage (dashed rectangle), initial RPE cell damage (solid line rectangle), RPE cell damage and initial MBF (dashed circle), ophthalmoscopically visible damage (solid line circle). The radiant exposures and the presence or absence of MBF detection as well as FA and ophthalmoscopic visibility are indicated in each subfigure.

0.49 for cell damage, $A_{MBF} = 124$ and $b_{MBF} = 0.64$ for MBF, and $A_{Opb} = 259$ and $b_{opb} = 0.51$ for values of τ in microseconds. The small colored points indicate local thresholds of individual spots in order to demonstrate the variability. $\bar{H}_{MBF}$ (blue points) was calculated from these data. It can be seen that some local (intraindividual) thresholds for MBF are below the mean (interindividual) thresholds for cell damage. Furthermore, there are some local (intraindividual) thresholds for MBF above the mean (interindividual) thresholds for ophthalmoscopic visibility during treatment.

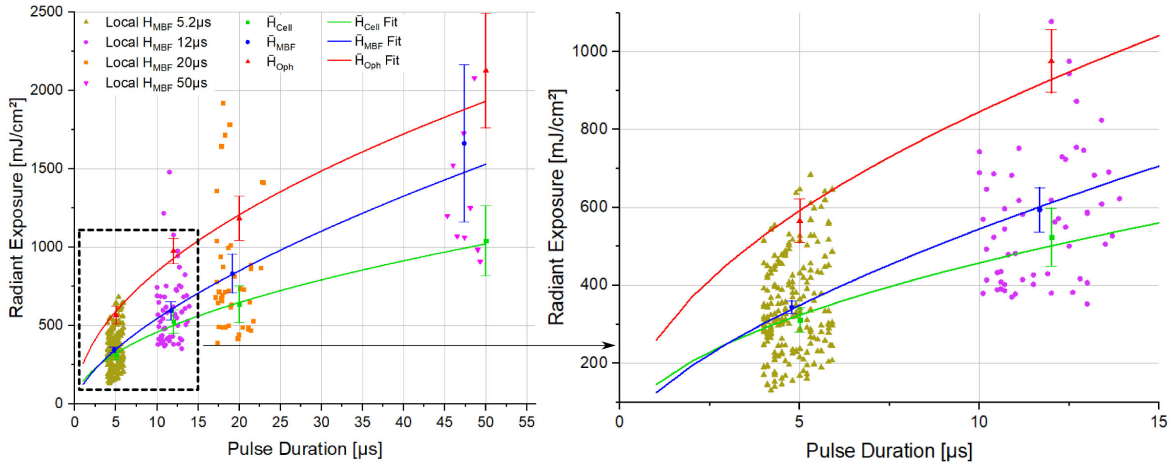

Figure 6. Threshold radiant exposures over pulse duration in vivo. *Small dots* represent local H_{MBF} values of individual spots. Points with *error bar* display interindividual (mean) threshold values of FA visible cell damage (*green rectangles*), MBF (*blue dots*), and ophthalmoscopic visibility (*red triangles*). *Lines* show a fit function. The *dashed area* is magnified in the *right plot*.

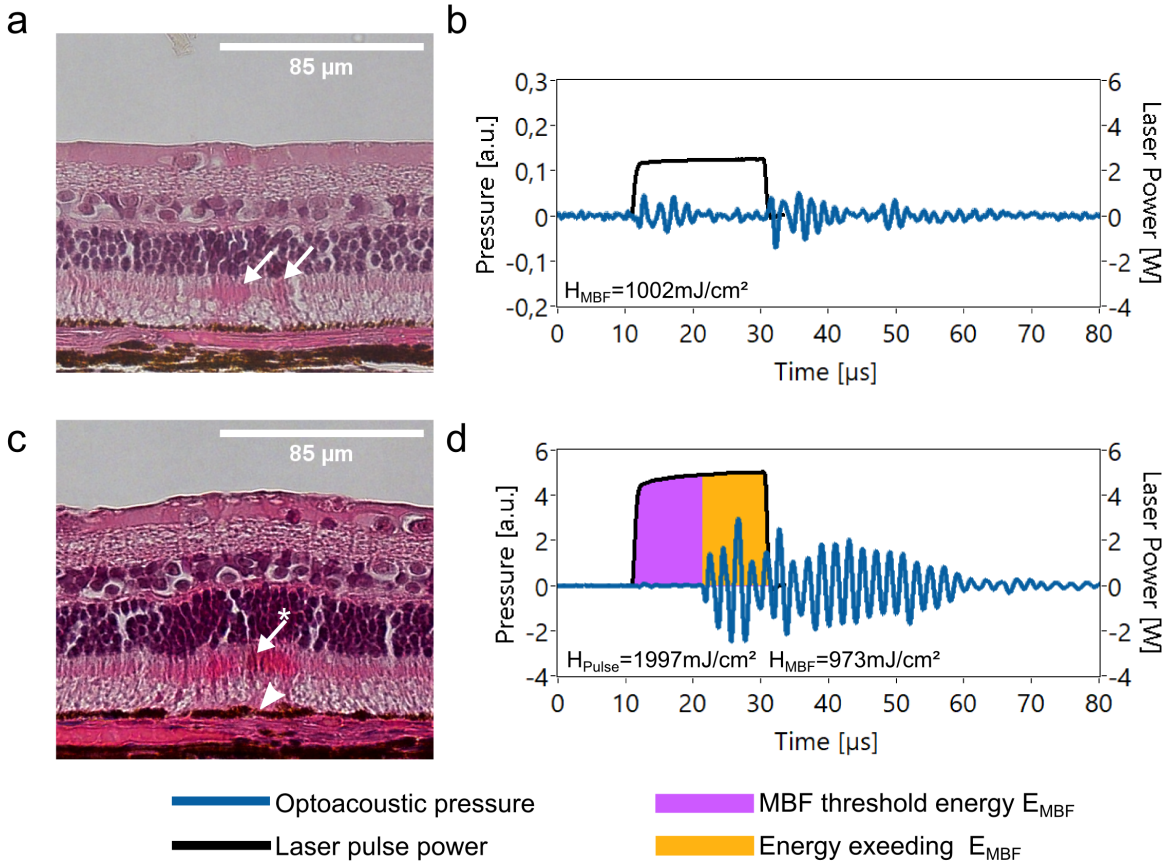

Figure 7. (**a**) HE-stained image of an ophthalmoscopically nonvisible region. A slightly stronger eosin staining in the photoreceptor inner segments is noticed (*arrows*). A maximal temperature of 79.5 ± 3.9°C was determined for this lesion from the transient. (**b**) Laser pulse and optoacoustic transient acquired during the irradiation process of the region displayed in (**a**); MBF was not detected. (**c**) HE-stained image of an ophthalmoscopically faintly visible region. Remarkable changes are an eosinophilic unstructured substance directly on the RPE (*arrowhead*), a stronger staining of eosin in the photoreceptor inner segments (*arrow*), and the deformation of a photoreceptor cell layer (*asterisk*). (**d**) Laser pulse and optoacoustic transient acquired during the irradiation process of the region displayed in subfigure c, revealing MBF.

Histology

Figure 7 shows representative results of HE staining of a rabbit retina at two different irradiated sites with corresponding optoacoustic (OA) transients and power of a 20-µs laser pulse applied. Figure 7a presents an irradiated region that did not show MBF (Fig. 7b) and was ophthalmoscopically not visible with $H_{pulse} = 1002\,\mathrm{mJ/cm^2}$. Although

there is almost no remarkable morphologic alteration, a stronger staining of eosin (pink color) can be observed in the photoreceptor inner/outer segment layers (Fig. 7a, arrows). Figure 7c displays a region where ophthalmoscopically very faint change was observed with $H_{pulse} = 1997\,mJ/cm^2$. The OA transient shows apparent MBF after 10 µs with $H_{MBF} = 973\,mJ/cm^2$ (Fig. 7d). Slight destructive changes are indicated by the following findings: an eosinophilic unstructured substance directly on the RPE (Fig. 7c, arrowhead), a pronounced eosin staining in the photoreceptor inner segments (Fig. 7c, arrow), and the deformation of a photoreceptor cell layer (Fig. 7c, asterisk).

Discussion

The application of lasers to the treatment of retinal diseases, especially macular diseases, has been attracting increasing attention again in recent years. Different from the photocoagulation that involves photoreceptor damage, treatment with RPE selective destruction (thermomechanical effect) or hyperthermia (mild thermal effect) can lead to a therapeutic effect without causing central scotoma. Thus, it is applicable solely or as an adjunct therapy of pharmaceutical treatments such as an intravitreal injection of anti-VEGF. There is increasing clinical evidence for the effectiveness of these laser treatments.[14–19,35–38] Thus, a laser system that enables one to choose the treatment modality properly according to the purpose, selective RPE destruction, mild hyperthermia, or classical photocoagulation with desired strength is very useful. Moreover, it would be also highly valuable to have a method that can monitor and display the tissue response during treatment sensitively.

In this work, the irradiation thresholds for RPE damage ex vivo and in vivo were investigated with respect to the pulse duration in the 2-µs to 50-µs range using a 15-W diode laser, representing new upcoming high-power laser systems with fairly uniform radiant exposure across the beam profile. The microsecond pulse duration range, including the transition from thermal to thermomechanical effects, has been little investigated so far. An overview is given by Schüle et al.[11] for RPE damage thresholds in vitro over the range from 5 µs to 3 ms, but without sampling points between 5 and 50 µs.

In order to discriminate thermal and thermomechanical damage, we evaluated optoacoustic pressure waves emitted from the RPE during laser irradiation with high time resolution. The start and end of the laser pulse are both demarked by weak thermoelastic acoustic transients originating from the onset of heating and cooling, respectively. Interestingly, the transient related to the cooling phase is always larger than the one of the heating phase. This reflects the higher tissue temperature at the end of the pulse and consequently the stronger pressure wave due to the higher Grüneisen coefficient in the beginning of the cooling phase.[5] Considering the pressure amplitudes and/or frequencies of the transients as well as the laser pulse shape allows one to quantify the temperature rise in the irradiated volume. For example, the maximal temperature for the lesion shown in histology (Fig. 7a) was determined to 79.5 ± 3.9°C. A detailed description and evaluation of temperature measurements and temperature-related cell damage in the microsecond time domain exceed the scope of this work and will become subject of a separate paper. At higher irradiance, a third transient with an amplitude up to two orders in magnitude higher than the thermoelastic ones is observed prior to the cooling transient, which can be attributed to MBF. Measuring the point in time microbubbles nucleate allows one to determine the threshold energy for MFB with so far unmatched precision and demonstrates its contribution of photodisruption to the cellular damage. Although this optoacoustic detection method is very sensitive, it cannot be ruled out that the occurrence of very small, nanometer-sized bubbles will not be detected. However, these bubbles are unlikely to cause cell disruption.

An important factor that needs to be taken into account for retinal laser irradiation in the nanosecond to microsecond time range are the intensity fluctuations across the beam profile. The intensity modulations originate from the limited number of interfering modes in multimode optical fibers and depend on the coherence length and wavelength of the laser light as well as the length, diameter, and numerical aperture of the optical transmission fiber used. In order to achieve uniform tissue effects, these fluctuations should be kept small, which especially counts for pulse durations of microseconds or lower where thermal diffusion does not level spatial temperature peaks. To quantify the intensity modulations, the factor IMF was introduced, giving the peak to average ratio. The beam profile of the current system was fairly uniform (Fig. 1) with an IMF around 1.2, and strong random intensity fluctuations were not observed. This is in contrast to previous work from Schüle et al.,[11] who used an $Argon^+$ laser with high coherence length and thus a high IMF of 3.8. Consequently, their reported threshold data not considering the IMF are much lower than those from this study with threshold radiant exposures in vitro of 465 and $1198\,mJ/cm^2$ for H_{Cell} and 496 and $1770\,mJ/cm^2$ for H_{MBF} for a 5.2- and 50-µs pulse, respectively. The logarithmic increase over pulse duration is related to increasing heat flow during the irradiation until the relevant temperatures for tissue effects are achieved.

A most interesting point is the type of damage and the DR associated with the different pulse durations. With regard to thermal damage, it is well known that the DR decreases with decreasing pulse durations, owing to reduced heat diffusion.[11] If the pulse becomes shorter and shorter, one might hypothesize that eventually only the RPE might be damaged selectively by thermal effects due to the heated intracellular melanosomes.[8,39] However, the shorter the heating time, the higher the temperatures need to be for denaturation, according to the Arrhenius theory. In rabbits, ED50 temperatures between 60°C and 65°C for barely visible lesions were measured by optoacoustics for pulse durations of 30 ms to 70 ms, between 55°C and 60°C for 100 and 200 ms, 50°C for 300 ms, and 48°C for 400 ms, respectively.[40] Further, highly sensitive OCT was performed in order to classify different lesion strengths in correlation to the temperatures achieved.[6] In a clinical study on patients with diabetic macula edema (DME), this classification was adopted. In OCT class 2, typically 50% of the lesions become visible at average temperatures of 75°C, 64°C, and 65°C for irradiation times of 20, 50, and 200 ms, respectively, on a 300-µm irradiation spot.[6] For the microsecond time domain, the temperature rise over the pulse can be evaluated from the ratio of the pressure peaks as discussed above. However, the coagulation temperatures in the µs time region are very close to the vaporization temperatures. Different studies showed the onset of vaporization at melanosomes around 140°C for a 1.8-µs pulse duration.[10] In case of intracellular melanosomes, the transient growth and collapse of the microbubbles lead to

Investigative Ophthalmology & Visual Science

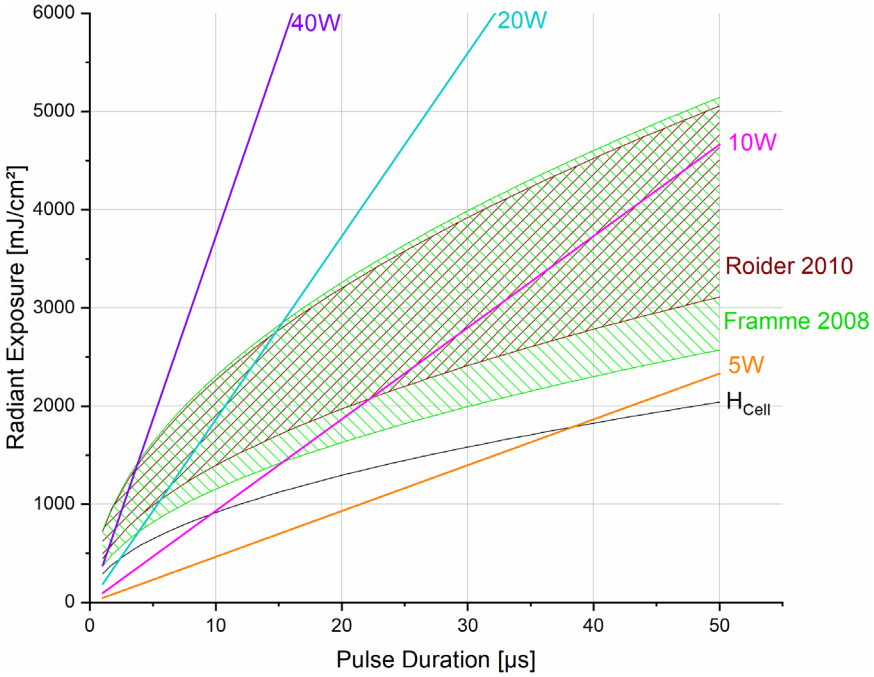

Figure 8. Extrapolated clinical radiant exposure ranges (*dashed areas*; for details, refer to the text) over pulse duration for SRT on patients with diabetic macula edema (DME) from Roider et al.[14] and Famme et al.[44] The *colored lines* are the powers that are required for the different pulse durations to achieve selective RPE effects on a spot diameter of 128 µm.

cell disruption[7,13] and can be described as a thermomechanical damage. This leads to selective RPE disintegration in case of SRT when irradiance is kept close above MBF threshold.

When using a 5-µs pulse duration, Schüle et al.[11] still observed MBF-related cell death, a mixed damage effect at 50 µs, and pure thermal damage dominating at 500 µs. Lee et al.[12] found thresholds for cell damage and MBF to be approximately equal for pulses up to 10 µs. At 20 µs, they found the cell damage threshold to be 10% lower than the MBF threshold, which is close to the approximately 20% we found in this work at 20 µs.[12] Other ex vivo experiments with optical microbubble detection using a scanned laser beam reported predominant microbubble-induced cell damage up to 20 µs in bovine eyes.[12,41] Another study making use of optical microbubble detection reported that H_{MBF} was 10% higher than $\bar{H}_{Cell}$ at 6 µs,[42] which is also very close to our data (DR of 1.07 and 1.11 for ex vivo and in vivo data at 5 µs). For a pulse duration of 5 µs, thermal coagulation has been predicted by one study[8] but using repetitive exposure. As shown in this work, the threshold DR, $\bar{H}_{MBF}$ to $\bar{H}_{Cell}$, approaches 1 toward shorter pulses. This means that further confining and reducing the thermal damage range by using shorter pulses is limited by the occurrence of microbubbles. The DR indicating pure thermal effects without detectable MBF drops from 1.48 ex vivo (1.60 in vivo) to 1.07 (1.11) for pulse durations of 50 to 5.2 µs, respectively. For a pulse duration of 2 µs, the difference between $\bar{H}_{Cell}$ $(259\,\mathrm{mJ/cm^2})$ and $\bar{H}_{MBF}$ $(257\,\mathrm{mJ/cm^2})$ is less than 1% of $\bar{H}_{Cell}$ $(2\,\mathrm{mJ/cm^2})$. This difference was not statistically significant. In summary and under consideration of the varying RPE absorption, it is almost impossible to target at pure thermal damage with pulse durations below 50 µs, under avoidance of MBF, without technical assistance. However, an accurate automatic feedback system controlling the laser output in real time might help to avoid MBF.

The results of the in vivo experiments also suggest that the damage ratio increases nonlinearly with pulse duration. Thus, thermal cell damage is likely the primary cell damage mechanism just at threshold radiant exposure, but MBF sets in with slightly higher energy, and mechanical damage is superimposed. The histologic images of HE staining shown in the current study also suggest the possible thermal effect next to MBF. A mildly increased eosin staining shown at the site without detectable MBF may suggest the occurrence of some sort of thermal impact. Since eosinophilic cell organelles include mitochondria and proteins,[43] the increased eosin staining may reflect from sublethal thermal impact, such as the increased metabolic activity, to lethal damage. Further histologic investigations are required in future studies to obtain more information on the local damage range and appearance originating from thermal and mechanical effects in dependence of the pulse duration and radiant exposure.

In case high-power lasers are used to address RPE effects as selective as possible, such as in SRT, it is recommended to use the shortest possible pulse duration with which the threshold of cell damage can be obtained. Owing to the strong light scattering in older human eyes, the thresholds for RPE damage were found to be 2.5 to 5.0 times larger than those for rabbits at a pulse duration of 1.7 µs. Using a spot diameter of 200 µm, Roider et al.[14] reported a mean threshold range from 200 to 325 µJ in patients with diabetic macula edema. Framme et al.[44] published thresholds in the range from 150 to 300 µJ in patients with central serous retinopathy. Extrapolating theses clinical data, Figure 8 displays the estimated required laser power for 5 W to 40 W (solid lines) to achieve RPE damage on a spot diameter of 128 µm in clinical settings.[14,44] However, thermal effects not solely on the RPE but also on the photoreceptors, Bruch's membrane, and choroidea need to be considered above pulse durations of 2 µs.

With respect to control the laser effects in clinical applications, an automatic real-time controlled laser system is recommended. However, as the power is limited, it is useful to apply the maximum power and cease laser emission after the point in time the MBF threshold has passed. For an MBF-related real-time control of the treatment, the optoacoustic approach presented here is not suited owing to the almost 20 µs of acoustic transit time of the pressure wave to the cornea. Therefore, either a pulse series with increasing pulse duration and acoustic control or an optical approach as shown by reflectometry is demanded.[24]

In conclusion, high average power lasers offer achievement of thermal or thermomechanical effects at the retina by choosing the appropriate pulse duration. All standard application modes can be addressed by just one laser system: classical LPC with pulse durations >10 ms, micropulsing[29,36,45,46] using repetitive pulses of 100 to 300 µs (duty cycle of 5%–15% at a repetition rate of 500 Hz), and very confined damage ranges around the RPE coming close to SRT using low microsecond pulse durations.

Acknowledgments

The authors thank A.R.C. for supplying the laser system and the German Ministry of Research and Technology for supporting the research project (BMBF Grant #13N14443, #13N14444 and, #13N14445, alliance MetaNetz).

Disclosure: **E. Seifert**, None; **S.R. Sonntag**, None; **P. Kleingarn**, None; **D. Theisen-Kunde**, None; **S. Grisanti**, None; **R. Birngruber**, None; **Y. Miura**, None; **R. Brinkmann**, None

References

1. Gabel V-P, Birngruber R, Hillenkamp F. Visible and near infrared light absorption in pigment epithelium and choroid. *Proc 23rd Consilium Ophthalmologicum Kyoto Excerpta Medica*. 1978;450:658–662.
2. Birngruber R, Hillenkamp F, Gabel V-P. Theoretical investigations of laser thermal retinal injury. *Health Physics*. 1985;48:781–796.
3. Wang J, Quan Y, Dalal R, Palanker D. Comparison of continuous-wave and micropulse modulation in retinal laser therapy. *Invest Ophthalmol Vis Sci*. 2017;58:4722–4732.
4. Denton ML, Noojin GD, Foltz MS, et al. Spatially correlated microthermography maps threshold temperature in laser-induced damage. *J Biomed Opt*. 2011;16:036003.
5. Brinkmann R, Koinzer S, Schlott K, et al. Real-time temperature determination during retinal photocoagulation on patients. *J Biomed Opt*. 2012;17:0612191–06121910.
6. Koinzer S, Schlott K, Portz L, et al. Correlation of temperature rise and optical coherence tomography characteristics in patient retinal photocoagulation. *J Biophotonics*. 2012;5:889–902.
7. Brinkmann R, Huettmann G, Roegener J, Roider J, Birngruber R, Lin CP. Origin of retinal pigment epithelium cell damage by pulsed laser irradiance in the nanosecond to microsecond time regimen. *Lasers Surg Med*. 2000;27:451–464.
8. Roider J, Hillenkamp F, Flotte T, Birngruber R. Microphotocoagulation: selective effects of repetitive short laser pulses. *Proc Natl Acad Sci USA*. 1993;90:8643–8647.
9. Neumann J, Brinkmann R. Nucleation dynamics around single microabsorbers in water heated by nanosecond laser irradiation. *J Appl Phys*. 2007;101:114701.
10. Neumann J, Brinkmann R. Boiling nucleation on melanosomes and microbeads transiently heated by nanosecond and microsecond laser pulses. *J Biomed Opt*. 2005;10:024001–02400112.
11. Schüle G, Rumohr M, Huettmann G, Brinkmann R. RPE damage thresholds and mechanisms for laser exposure in the microsecond-to-millisecond time regimen. *Invest Ophthalmol Vis Sci*. 2005;46:714–719.
12. Lee H, Alt C, Pitsillides CM, Lin CP. Optical detection of intracellular cavitation during selective laser targeting of the retinal pigment epithelium: dependence of cell death mechanism on pulse duration. *J Biomed Opt*. 2007;12:064034.
13. Neumann J, Brinkmann R. Cell disintegration by laser-induced transient microbubbles and its simultaneous monitoring by interferometry. *J Biomed Opt*. 2006;11:041112.
14. Roider J, Liew SHM, Klatt C, et al. Selective retina therapy (SRT) for clinically significant diabetic macular edema. *Graefes Arch Clin Exp Ophthalmol*. 2010;248:1263–1272.
15. Framme C, Walter A, Prahs P, et al. Structural changes of the retina after conventional laser photocoagulation and selective retina treatment (SRT) in spectral domain OCT. *Curr Eye Res*. 2009;34:568–579.
16. Klatt C, Elsner H, Porksen E, et al. Selective retina therapy in central serous chorioretinopathy with detachment of the pigmentary epithelium. *Ophthalmologe*. 2006;103:850–855.
17. Yasui A, Yamamoto M, Hirayama K, et al. Retinal sensitivity after selective retina therapy (SRT) on patients with central serous chorioretinopathy. *Graefes Arch Clin Exp Ophthalmol*. 2017;255:243–254.
18. Park YG, Kang S, Kim M, Yoo N, Roh YJ. Selective retina therapy with automatic real-time feedback-controlled dosimetry for chronic central serous chorioretinopathy in Korean patients. *Graefes Arch Clin Exp Ophthalmol*. 2017;255:1375–1383.
19. Kang S, Park YG, Kim JR, et al. Selective retina therapy in patients with chronic central serous chorioretinopathy: a pilot study. *Medicine (Baltimore)*. 2016;95:e2524.
20. Guymer RH, Wu Z, Hodgson LAB, et al. Subthreshold nanosecond laser intervention in age-related macular degeneration: the LEAD randomized controlled clinical trial. *Ophthalmology*. 2019;126:829–838.
21. Framme C, Schüle G, Roider J, Birngruber R, Brinkmann R. Influence of pulse duration and pulse number in selective RPE laser treatment. *Lasers Surg Med*. 2004;34:206–215.
22. Roider J, El Hifnawi E, Birngruber R. Bubble formation as primary interaction mechanism in retinal laser exposure with 200-ns laser pulses. *Lasers Surg Med*. 1998;22:240–248.
23. Schüle G, Elsner H, Framme C, Roider J, Birngruber R, Brinkmann R. Optoacoustic real-time dosimetry for selective retina treatment. *J Biomed Opt*. 2005;10:064022.
24. Seifert E, Tode J, Pielen A, et al. Selective retina therapy: toward an optically controlled automatic dosing. *J Biomed Opt*. 2018;23:1–12.
25. Park Y-G, Seifert E, Roh YJ, Theisen-Kunde D, Kang S, Brinkmann R. Tissue response of selective retina therapy by means of a feedback-controlled energy ramping mode. *Clin Exp Ophthalmol*. 2014;42:846–855.
26. Steiner P, Ebneter A, Berger LE, et al. Time-resolved ultrahigh resolution optical coherence tomography for real-time monitoring of selective retina therapy. *Invest Ophthalmol Vis Sci*. 2015;56:6654–6662.
27. Burri C, Hutfilz A, Grimm L, et al. Optical coherence tomography controlled selective retina therapy with a novel microsecond laser. In: *European Conference on Biomedical Optics*. Munich, Germany: SPIE Proceedings (Optical Society of America); 2019:1107903-1–1107903-6.
28. Povazay B, Brinkmann R, Stoller M, Kessler R. Selective retina therapy. In: Bille JF, ed. *High Resolution Imaging in*

Microscopy and Ophthalmology: New Frontiers in Biomedical Optics. Cham, Switzerland: Springer; 2019:237–259.

29. Luttrull JK, Dorin G. Subthreshold diode micropulse laser photocoagulation (SDM) as invisible retinal phototherapy for diabetic macular edema: a review. *Curr Diabetes Rev*. 2012;8:274–284.
30. Luttrull JK, Sramek C, Palanker D, Spink CJ, Musch DC. Long-term safety, high-resolution imaging, and tissue temperature modeling of subvisible diode micropulse photocoagulation for retinovascular macular edema. *Retina*. 2012;32:375–386.
31. Lavinsky D, Sramek C, Wang J, et al. Subvisible retinal laser therapy: titration algorithm and tissue response. *Retina*. 2014;34:87–97.
32. Birngruber R, Drechsel E, Hillenkamp F, Gabel VP. Minimal spot size on the retina formed by the optical system of the eye. *Int Ophthalmol*. 1979;1:175–178.
33. Birngruber R, Gabel V-P, Hillenkamp F. Experimental studies of laser thermal retinal injury. *Health Phys*. 1983;44:519–531.
34. Borland RG, Brennan DH, Marshall J, Viveash JP. The role of fluorescence angiography in the detection of laser-induced damage to the retina: a threshold study for Q-switched, neodymium and ruby lasers. *Exp Eye Res*. 1978;27:471–493.
35. Inagaki K, Hamada M, Ohkoshi K. Minimally invasive laser treatment combined with intravitreal injection of antivascular endothelial growth factor for diabetic macular oedema. *Sci Rep*. 2019;9:7585.
36. Scholz P, Altay L, Fauser S. A review of subthreshold micropulse laser for treatment of macular disorders. *Adv Ther*. 2017;34:1528–1555.
37. Moisseiev E, Abbassi S, Thinda S, Yoon J, Yiu G, Morse LS. Subthreshold micropulse laser reduces anti-VEGF injection burden in patients with diabetic macular edema. *Eur J Ophthalmol*. 2018;28:68–73.
38. Luttrull JK, Sinclair SH, Elmann S, Glaser BM. Low incidence of choroidal neovascularization following subthreshold diode micropulse laser (SDM) in high-risk AMD. *PLoS One*. 2018;13:e0202097.
39. Roider J, Michaud NA, Flotte TJ, Birngruber R. Response of the retinal pigment epithelium to selective photocoagulation. *Arch Ophthalmol*. 1992;110:1786–1792.
40. Schlott K, Koinzer S, Ptaszynski L, et al. Automatic temperature controlled retinal photocoagulation. *J Biomed Opt*. 2012;17:0612231–0612238.
41. Alt C, Framme C, Schnell S, Lee H, Brinkmann R, Lin CP. Selective targeting of the retinal pigment epithelium using an acousto-optic laser scanner. *J Biomed Opt*. 2005;10:064014.
42. Roegener J, Brinkmann R, Lin CP. Pump-probe detection of laser-induced microbubble formation in retinal pigment epithelium cells. *J Biomed Opt*. 2004;9:367–371.
43. Chan JK. The wonderful colors of the hematoxylin-eosin stain in diagnostic surgical pathology. *Int J Surg Pathol*. 2014;22:12–32.
44. Framme C, Walter A, Prahs P, Theisen-Kunde D, Brinkmann R. Comparison of threshold irradiances and online dosimetry for selective retina treatment (SRT) in patients treated with 200 nanoseconds and 1.7 microseconds laser pulses. *Lasers Surg Med*. 2008;40:616–624.
45. Su D, Hubschman JP. A review of subthreshold micropulse laser and recent advances in retinal laser technology. *Ophthalmol Ther*. 2017;6:1–6.
46. Brader HS, Young LH. Subthreshold diode micropulse laser: a review. *Semin Ophthalmol*. 2016;31:30–39.